

**IRON OXIDE ENCAPSULATED GOLD  
COLLOIDAL NANOPARTICLE VIA RAPID  
SONOCHEMICAL METHOD FOR MRI AND CT  
IMAGING APPLICATION**

**MOHAMMED ALI DHEYAB**

**UNIVERSITI SAINS MALAYSIA**

**2021**

**IRON OXIDE ENCAPSULATED GOLD  
COLLOIDAL NANOPARTICLE VIA RAPID  
SONOCHEMICAL METHOD FOR MRI AND CT  
IMAGING APPLICATION**

by

**MOHAMMED ALI DHEYAB**

**Thesis submitted in fulfilment of the requirements  
for the degree of  
Doctor of Philosophy**

**February 2021**

## ACKNOWLEDGEMENT

On this memorable day in my life, I reached the final destination of my journey as a PhD student; first of all, I would like to thank Almighty Allah for granting me health and patience to complete this research work.

Also, I am deeply thankful to my main supervisor, **Professor Dr. Azlan Abdul Aziz**, for his support, kind cooperation, useful contribution and valuable guidance throughout the course of this study. Thanks again, Prof. for having your door open every time I needed help.

I express appreciation to the staff of the Nano-Optoelectronics Research and Technology Laboratory (NOR lab) and Institute for Research in Molecular Medicine (INFORMM lab) assistants for technical assistance during my laboratory work, particularly in the sample characterizations.

My heartfelt gratitude also goes to my family members: to my father, mother, brothers, sisters and friends for their continuous prayers and support. Finally, I thank all who supported me in any respect during the completion of this study.

**Mohammed Ali Dheyab**

## TABLE OF CONTENTS

<b>ACKNOWLEDGEMENT</b> .....	<b>ii</b>
<b>TABLE OF CONTENTS</b> .....	<b>iii</b>
<b>LIST OF TABLES</b> .....	<b>viii</b>
<b>LIST OF FIGURES</b> .....	<b>ix</b>
<b>LIST OF SYMBOLS</b> .....	<b>xiv</b>
<b>LIST OF ABBREVIATIONS</b> .....	<b>xv</b>
<b>LIST OF APPENDICES</b> .....	<b>xviii</b>
<b>ABSTRAK</b> .....	<b>xix</b>
<b>ABSTRACT</b> .....	<b>xx</b>
<b>CHAPTER 1 INTRODUCTION</b> .....	<b>1</b>
1.1 History of Nanotechnology .....	1
1.2 Iron Oxide Nanoparticles (Fe <sub>3</sub> O <sub>4</sub> NPs) .....	2
1.3 Core@shell Nanoparticles (Fe <sub>3</sub> O <sub>4</sub> @Au NPs) .....	2
1.4 Problem statement .....	3
1.5 Objective of the study .....	5
1.6 Scope of the study .....	5
1.7 Contribution of the study.....	6
1.8 Organization of the thesis.....	6
<b>CHAPTER 2 LITERATURE REVIEW</b> .....	<b>7</b>
2.1 A brief overview of iron oxide nanoparticles.....	7
2.2 Wet chemical methods for the synthesis of magnetite nanoparticles.....	7
2.2.1 Co-precipitation method.....	8
2.2.2 Electrochemical method.....	10
2.2.3 Hydrothermal method .....	10
2.2.4 Microemulsions and reverse micelles method .....	12

2.2.5	Sol-gel method .....	14
2.2.6	Solvothermal method .....	15
2.2.7	Sonication method.....	16
2.2.8	Thermal decomposition method.....	16
2.3	Surface modification of Fe <sub>3</sub> O <sub>4</sub> NPs .....	21
2.3.1	Inorganic coating.....	21
2.3.1(a)	Gold .....	21
2.3.1(b)	Silica .....	23
2.3.2	Organic coating .....	24
2.3.2(a)	Chitosan .....	24
2.3.2(b)	Polyethylene Glycol (PEG) .....	25
2.3.2(c)	Polyvinyl Alcohol (PVA) .....	26
2.3.2(d)	Poly Vinyl Pyrrolidone (PVP).....	27
2.4	Synthesis of Fe <sub>3</sub> O <sub>4</sub> /Au Core/shell nanoparticles .....	28
2.4.1	Synthesis of a Fe <sub>3</sub> O <sub>4</sub> bi-layer structure.....	29
2.4.2	Synthesis Fe <sub>3</sub> O <sub>4</sub> /glue/Au multilayer.....	32
2.5	Effect of sonochemistry on coating Fe <sub>3</sub> O <sub>4</sub> @Au core@shell NPs.....	36
2.6	The role of Sodium Citrate .....	39
2.7	Fe <sub>3</sub> O <sub>4</sub> @Au NPs for dual-mode MRI and CT scan.....	40
2.8	Summary .....	44
<b>CHAPTER 3 THEORETICAL BACKGROUND.....</b>		<b>45</b>
3.1	Introduction .....	45
3.2	Theory of sonochemistry.....	45
3.3	Cavitation .....	46
3.4	Acoustic cavitation .....	47
3.5	Effects of cavitation .....	49
3.5.1	Physical effect .....	49

3.5.2	Chemical effect .....	50
3.5.3	Thermal effect .....	51
3.6	Effects of Sonochemistry on stability .....	51
3.7	Magnetic properties of Fe <sub>3</sub> O <sub>4</sub> NPs.....	52
3.8	Ionic properties of Au NPs.....	54
3.9	Response Surface Methodology (RSM).....	55
3.10	Theory of Magnetic Resonance Imaging (MRI) .....	57
3.10.1	T <sub>1</sub> Relaxation Time .....	61
3.10.2	T <sub>2</sub> Relaxation Time .....	62
3.11	Theory of Computed Tomography (CT-Scan).....	64
3.12	MRI and CT-Scan Contrast Agent .....	65
3.13	Summary .....	68
<b>CHAPTER 4 METHODOLOGY AND OPTIMIZATION .....</b>		<b>69</b>
4.1	Introduction .....	69
4.2	Chemicals .....	69
4.3	Characterization .....	70
4.4	Synthesis of Fe <sub>3</sub> O <sub>4</sub> NPs .....	70
4.5	Synthesis of Au NPs using sonochemical method .....	73
4.6	Synthesis of Fe <sub>3</sub> O <sub>4</sub> @Au NPs .....	74
4.7	Model Development for Fe <sub>3</sub> O <sub>4</sub> Au NPs using sonochemical method .....	75
4.7.1	Design of Experiment using RSM .....	75
4.7.2	Significance of the independent variables of the Zeta potential for synthesised Fe <sub>3</sub> O <sub>4</sub> @Au NPs.....	77
4.8	Characterization of Fe <sub>3</sub> O <sub>4</sub> @Au NPs .....	78
4.8.1	X-Ray Diffraction (XRD) .....	78
4.8.2	Ultraviolet – visible spectroscopy (UV – vis).....	81
4.8.3	Transmission Electron Microscopy (TEM) .....	82
4.8.4	Field emission scanning electron microscopy (FESEM).....	84

4.8.5	Energy dispersive x-ray (EDX).....	86
4.8.6	Zetasizer .....	87
4.8.7	Vibrating Sample Magnetometer (VSM).....	90
4.9	The Fe <sub>3</sub> O <sub>4</sub> @Au concentration measurement .....	91
4.10	The cytotoxicity assay for Fe <sub>3</sub> O <sub>4</sub> and Fe <sub>3</sub> O <sub>4</sub> @Au.....	92
4.11	Fe <sub>3</sub> O <sub>4</sub> @Au for dual-mode MRI and CT scan .....	94
4.12	Summary .....	96
<b>CHAPTER 5 PHYSIOCHEMICAL PROPERTIES OF THE OPTIMIZED Fe<sub>3</sub>O<sub>4</sub>@Au NPs AND THEIR MEDICAL APPLICATION .....</b>		<b>97</b>
5.1	Introduction .....	97
5.2	Response surface plots for Fe <sub>3</sub> O <sub>4</sub> @Au NPs.....	97
5.3	Effect of independent variables on zeta potential .....	99
5.4	Comparison of predicted and experimental results .....	101
5.5	Physical properties of Fe <sub>3</sub> O <sub>4</sub> @Au NPs .....	102
5.5.1	X-Ray Diffraction (XRD) .....	102
5.5.2	Ultraviolet–visible spectroscopy (UV–Vis).....	104
5.5.3	Transmission electrons Microscope (TEM) analysis.....	106
5.5.4	Field Emission Scanning Electron Microscopy (FESEM) Analysis.....	107
5.5.5	Energy-dispersive X-ray Spectroscopy (EDX) Analysis.....	109
5.6	Materials stability of Fe <sub>3</sub> O <sub>4</sub> @Au .....	110
5.7	Magnetic properties of Fe <sub>3</sub> O <sub>4</sub> @Au NPs.....	112
5.8	The cytotoxicity assay for Fe <sub>3</sub> O <sub>4</sub> and Fe <sub>3</sub> O <sub>4</sub> @Au in HEK-293 cells.....	113
5.9	Applications of Fe <sub>3</sub> O <sub>4</sub> @Au NPs for dual-mode MRI and CT scan.....	114
<b>CHAPTER 6 CONCLUSION AND FUTURE RECOMMENDATIONS....</b>		<b>117</b>
6.1	Conclusion.....	117
6.2	Recommendations for Future Research .....	119

**REFERENCES..... 120**

APPENDICES

LIST OF PUBLICATIONS

## LIST OF TABLES

	<b>Page</b>
Table 2.1	Comparison between synthesis methods in preparation Fe <sub>3</sub> O <sub>4</sub> ..... 19
Table 2.2	Comparison between various synthesis approach.....35
Table 2.3	Summary of the published articles on Fe <sub>3</sub> O <sub>4</sub> @Au core@shell NPs via sonochemical method.....39
Table 2.4	Summary of the published articles on core@shell NPs .....43
Table 4.1	Experimental matrix..... 76
Table 4.2	ANOVA results for zeta potential.....78
Table 5.1	Comparing the predicted and the experimental result..... 101
Table 5.2	Comparison of size nanoparticles measured by TEM and FESEM. 108
Table 5.3	Detailed elemental analysis of Fe <sub>3</sub> O <sub>4</sub> and Fe <sub>3</sub> O <sub>4</sub> @Au sample using EDX ..... 109

## LIST OF FIGURES

	<b>Page</b>
Figure 2.1	Various methods of producing Fe <sub>3</sub> O <sub>4</sub> and its surface modifications with organic and inorganic materials .....8
Figure 2.2	The formation of Fe <sub>3</sub> O <sub>4</sub> NPs by mixing two water-in-oil microemulsions, where reactant 1 contains salt or a complex of a metal, while reactant 2 contains a precipitating agent [82]..... 14
Figure 2.3	TEM images with different sizes and shapes of agglomerated Fe <sub>3</sub> O <sub>4</sub> depending on the method of synthesis (a) Co-precipitation [122] (b) Electrochemical [53] (c) Hydrothermal [62] (d) Microemulsion [70] (e) Sol-gel [123] (f) Solvothermal [91] (g) Sonication [124] (h) Thermal decomposition [125]..... 18
Figure 2.4	Reaction steps of preparation Fe <sub>3</sub> O <sub>4</sub> /SiO <sub>2</sub> core/shell nanoparticles by condensation and hydrolysis of sol-gel precursors like tetraethyl orthosilicate (TEOS) [147].....24
Figure 2.5	Schematic representation of two approaches for synthesis Au coated Fe <sub>3</sub> O <sub>4</sub> .....29
Figure 2.6	TEM images with different sizes and shapes of Fe <sub>3</sub> O <sub>4</sub> @Au depending on the conditions of the synthesis method (a) Fe <sub>3</sub> O <sub>4</sub> /Au nanoparticles bi-layer [177], (b) Fe <sub>3</sub> O <sub>4</sub> /PZS/Au [28], (c) Fe <sub>3</sub> O <sub>4</sub> /PB/Au [188], (d) Fe <sub>3</sub> O <sub>4</sub> /PANI/Au [194] and (e) Fe <sub>3</sub> O <sub>4</sub> /PEI/Au [186] multilayer .....34
Figure 3.1	Representation of sound frequency ranges, with a rough guide of some applications .....46
Figure 3.2	Summary of the acoustic cavitation phenomenon steps that occur under ultrasonic radiation.....49
Figure 3.3	Illustration of the mechanism of the sonochemistry treatment to break down the agglomerations of NPs .....52

Figure 3.4	Schematic illustration of the MRI system, where the main components are indicated [276] .....	58
Figure 3.5	Illustration of hydrogen nuclei with magnetic interaction (a) when there is no external magnetic field, each individual moment has its random orientation, and, as a group together, they show zero net magnetization, (b) when there is an external magnetic field, proton spins align themselves with the field into two groups, one parallel to the external field, and the other antiparallel. There is always, however, a slightly larger number of parallel spins than antiparallel spins at equilibrium and that results in a nonzero net magnetic moment, or magnetization vector, in the direction parallel to the applied external field [277] .....	59
Figure 3.6	Schematic illustration of relaxation procedure in the MRI. (1) The proton nuclei precess randomly (2) The total magnetic moment $M$ of the spin aligns parallel to the external magnetic field. (3) A pulsed RF is introduced and (4) consequently, $M_0$ flip away from $B$ to the XY plane. (5) When RF is tuned off, the spin diphase at a $T_2$ decay time and releases their absorbed energy, which is absorbed as MRI signal [278].....	60
Figure 3.7	This diagram illustrates the simultaneous magnetization of (a) $T_1$ relaxation and (b) $T_2$ relaxation after the RF pulse is turned off [279] .....	62
Figure 3.8	Comparing MRI with and without contrast agents (a) image is without contrast (b) image is with contrast agent [291].....	66
Figure 3.9	Schematic representation of TE and TR [292].....	66
Figure 4.1	Flowchart of synthesis $Fe_3O_4@Au$ NPs using sonochemical method for medical applications .....	72
Figure 4.2	These experimental setups and equipment were used to produce $Fe_3O_4@Au$ NPs .....	74
Figure 4.3	Photography displays different colours for as-synthesis (a) $Fe_3O_4$ NPs, (b) Au NPs and (c) $Fe_3O_4@Au$ NPs.....	75

Figure 4.4	Bragg's diffraction for X-Ray diffraction by crystal plane.....	79
Figure 4.5	XRD analysis of Fe <sub>3</sub> O <sub>4</sub> NPs [305] .....	80
Figure 4.6	UV-vis result of Au NPs [306] .....	81
Figure 4.7	Schematic diagram of 3600 spectrophotometer (Shimadzu) [307]....	82
Figure 4.8	The schematic diagram of transmission electron microscopy (TEM) system [308].....	83
Figure 4.9	TEM image of Fe <sub>3</sub> O <sub>4</sub> @Au NPs with scale of 50 nm [188].....	84
Figure 4.10	SEM image shows the morphology of Fe <sub>3</sub> O <sub>4</sub> @Au NPs with scale of 1 μm [35] .....	85
Figure 4.11	Schematic diagram of FEI Nova NanoSEM [311] .....	86
Figure 4.12	Schematic diagram of EDX- analyser [307] .....	87
Figure 4.13	Schematic diagram of zeta potential for nanoparticles [316].....	89
Figure 4.14	Zeta potential results of Fe <sub>3</sub> O <sub>4</sub> @Au NPs [311] .....	90
Figure 4.15	VSM analysis of Fe <sub>3</sub> O <sub>4</sub> at room temperature [317] .....	91
Figure 4.16	Standard curve of the concentrations (a) iron and (b) gold.....	92
Figure 4.17	Seeded HEK293 cells in a flat-bottomed 96-well plate (a) without Fe <sub>3</sub> O <sub>4</sub> NPs (b) with Fe <sub>3</sub> O <sub>4</sub> @Au NPs .....	93
Figure 4.18	Enzyme-linked immunosorbent assay (ELISA).....	94
Figure 4.19	Agarose phantom mixed with different concentrations of Fe <sub>3</sub> O <sub>4</sub> @Au NPs For MRI and CT imaging.....	95
Figure 5.1	Correlation between predicted and actual observed data from the 14 experimental results for zeta potential .....	98
Figure 5.2	Three-dimensional response surface and two-dimensional contour plots showing mutual interaction and individual effects of different variables on zeta potential of the synthesised Fe <sub>3</sub> O <sub>4</sub> @Au NPs (a, b) The response surface and contour plots of HAuCl <sub>4</sub> (mL) vs SC (mL) while keeping sonication amplitude constant, (c, d) the response surface and contour plots of inoculum sonication amplitude vs HAuCl <sub>4</sub> (mL) while keeping SC (mL), (e, f) the	

	response and contour plots of inoculum sonication amplitude vs SC (mL) while keeping H <sub>2</sub> AuCl <sub>4</sub> (mL) constant.....	100
Figure 5.3	Optimized ramps show the optimized values of H <sub>2</sub> AuCl <sub>4</sub> , SC and sonication amplitude for improving the zeta potential of Fe <sub>3</sub> O <sub>4</sub> @Au NPs .....	102
Figure 5.4	X-ray diffraction (XRD) patterns of (a) Fe <sub>3</sub> O <sub>4</sub> and (b) Fe <sub>3</sub> O <sub>4</sub> @Au NPs .....	104
Figure 5.5	UV–vis spectra of different colloidal suspensions (a) Fe <sub>3</sub> O <sub>4</sub> , (b) Au NPs and (c) Fe <sub>3</sub> O <sub>4</sub> @Au NPs .....	105
Figure 5.6	TEM images and size distribution histograms of (a), (c) Fe <sub>3</sub> O <sub>4</sub> and (b), (d) Fe <sub>3</sub> O <sub>4</sub> @Au NPs.....	107
Figure 5.7	FESEM images and size distribution histograms of (a), (c) Fe <sub>3</sub> O <sub>4</sub> and (b), (d) Fe <sub>3</sub> O <sub>4</sub> @Au NPs.....	108
Figure 5.8	Energy-dispersive X-ray (EDX) of (a) Fe <sub>3</sub> O <sub>4</sub> @Au NPs and (b) Fe <sub>3</sub> O <sub>4</sub> .....	109
Figure 5.9	EDX mapping image of sample Fe <sub>3</sub> O <sub>4</sub> @Au NPs. The bright spots show the distribution elements of Fe, Au, C and O .....	110
Figure 5.10	The stability measurement of as-synthesised nanoparticles using zeta potential (a) Fe <sub>3</sub> O <sub>4</sub> , (b) Au NPs and (c) Fe <sub>3</sub> O <sub>4</sub> @Au NPs .....	112
Figure 5.11	(a) Magnetization curve of superparamagnetic (no coercivity nor remanence) Fe <sub>3</sub> O <sub>4</sub> @Au NPs at room temperature, the magnetic attraction of Fe <sub>3</sub> O <sub>4</sub> @Au NPs (b) Fe <sub>3</sub> O <sub>4</sub> @Au NPs in solution state (c) magnetic attraction of Fe <sub>3</sub> O <sub>4</sub> @Au NPs towards a magnet .....	113
Figure 5.12	Biocompatibility test with different concentrations and incubation times (24, 48 and 72 h) (a) Fe <sub>3</sub> O <sub>4</sub> and (b) Fe <sub>3</sub> O <sub>4</sub> @Au NPs against the (HEK-293) cell line .....	114
Figure 5.13	(a) T <sub>2</sub> -weighted MR image with different Fe concentrations (0.1, 0.2, 0.3, 0.4 and 0.5 mg). (b) The linear fitting of 1/T <sub>2</sub> of the Fe <sub>3</sub> O <sub>4</sub> @Au CNPs with different Fe concentrations. (c) CT image	

of the Fe<sub>3</sub>O<sub>4</sub>@Au CNPs with different Au concentrations (1, 2, 3, 4 and 5 mg/ml). (d) x-ray attenuation intensity..... 116

## LIST OF SYMBOLS

$^{\circ}\text{C}$	Degree Celsius
Oe	Oersted (magnetizing field)
Hc	Coercivity
$\mu\text{l}$	Microliter
$\theta$	Angle
$\lambda$	wavelength
$\omega_0$	Larmor frequency
$\zeta$	Zeta potential
$B_0$	magnetic field
$d_{hkl}$	interplanar spacing
$D_p$	Crystal size
$\varepsilon$	The strain
a	Lattice constant
h,k,l	Miller indices
$\gamma$	gyromagnetic ratio
Hz	Hertz
rpm	revolution per minutes
a.u	arbitrary unit

## LIST OF ABBREVIATIONS

Mr	Remanence
Ms	Saturation magnetization
APTES	(3-Aminopropyl)triethoxysilane
VSM	A vibrating-sample magnetometer
COOH	Carboxylate group
T <sub>2</sub>	Longitudinal Relaxation Time
r <sub>1</sub>	Transverse Relaxation rate
r <sub>2</sub>	Longitudinal Relaxation rate
DLS	Dynamic Light Scattering
TR	Repetition Time
TE	Echo time
T <sub>1</sub>	Transverse Relaxation Time
ppm	parts per million
Fe <sup>3+</sup>	Ferric
Fe <sup>2+</sup>	Ferrous
FTIR	Fourier-Transform Infrared Spectroscopy
FeO(OH)	Goethite
α-Fe <sub>2</sub> O <sub>3</sub>	Hematite
HCl	Hydrochloric acid
OH	Hydroxyl group
Fe(acac) <sub>3</sub>	Iron acetylacetonate
IONPs	Iron oxide nanoparticles
Fe(CO) <sub>5</sub>	Iron pentacarbonyl
FeCl <sub>2</sub>	Iron(II) chloride

FeCl <sub>3</sub>	Iron(III) chloride
γ-Fe <sub>2</sub> O <sub>3</sub>	Maghemite
MNPs	Magnetic nanoparticles
MRI	Magnetic Resonance Imaging
CT	Computed tomography
HU	Hounsfield Unit
NPs	Nanoparticles
Fe <sub>3</sub> O <sub>4</sub>	Magnetite
Au	Gold
MW	Molecular Weight
O/W	Oil-in-Water
PDI	Polydispersity Index Values
PEG	Polyethylene glycol
PVP	Polyvinylpyrrolidone
pH	Potential of Hydrogen
RF	Radio Frequency
NaCl	Sodium chloride
NaOH	Sodium hydroxide
SPIONs	Superparamagnetic Iron Oxide Nanoparticles
TEM	Transmission Electron Microscopy
H <sub>2</sub> O	Water
W/O	Water-in-Oil
XAFS	X-ray Absorption Fine Structure
XANES	X-ray Absorption Near Edge Structure
XRD	X-ray Diffraction
Adj. R <sup>2</sup>	Adjusted R – squared
Adeq. Pres.	Adequate precision

ANOVA	Analysis of variance
CCD	Central Composite Design
EDX	Energy-dispersive X-ray spectroscopy
FESEM	Field emission scanning electron microscopy
HAuCl <sub>4</sub>	Tetrachloroauric acid
HEK	Human embryonic kidney
NIR	Near-infra red
Pred. R <sup>2</sup>	Predicted R- squared
Prob.	Probability
RSM	Response Surface Methodology
SPR	Surface plasma resonance
UV-vis	Ultraviolet – visible spectroscopy
WST – 1	Water soluble tetrazolium - 1

## LIST OF APPENDICES

Appendix A1	T <sub>2</sub> weighted image of Fe <sub>3</sub> O <sub>4</sub> @Au NPs at TE 10 and TR 1000
Appendix A2	T <sub>2</sub> weighted image of Fe <sub>3</sub> O <sub>4</sub> @Au NPs at TE 15 and TR 1000
Appendix A3	T <sub>2</sub> weighted image of Fe <sub>3</sub> O <sub>4</sub> @Au NPs at TE 20 and TR 1000
Appendix A4	T <sub>2</sub> weighted image of Fe <sub>3</sub> O <sub>4</sub> @Au NPs at TE 30 and TR 1000
Appendix A5	T <sub>2</sub> weighted image of Fe <sub>3</sub> O <sub>4</sub> @Au NPs at TE 60 and TR 1000
Appendix A6	T <sub>2</sub> weighted image of Fe <sub>3</sub> O <sub>4</sub> @Au NPs at TE 120 and TR 1000
Appendix A7	T <sub>2</sub> weighted image of Fe <sub>3</sub> O <sub>4</sub> @Au NPs at TE 200 and TR 1000
Appendix B	CT image of Fe <sub>3</sub> O <sub>4</sub> @Au NPs at LEVEL: 40 HU, WINDOW: 120 HU

**NANOPARTIKEL TERKAPSUL FERUM OKSIDA KOLOIDAL EMAS  
MELALUI KAEDAH SONOKIMIA PANTAS UNTUK APLIKASI MRI DAN  
PENGIMEJAN CT**

**ABSTRAK**

Nanopartikel teras @ cengkerang ( $\text{Fe}_3\text{O}_4@Au$  NP) mempunyai pelbagai fungsi yang diperoleh dalam satu entiti stabil dan oleh itu telah diselidiki secara meluas. Walau bagaimanapun, kaedah langsung konvensional untuk sintesis  $\text{Fe}_3\text{O}_4@Au$  NPs sukar dan memakan masa. Oleh itu, kajian ini menyajikan teknik sonokimia yang mudah dan pantas untuk mensintesis  $\text{Fe}_3\text{O}_4@Au$  NP dengan sifat fizikokimia yang sangat baik untuk pengimejan resonans magnetik (MRI) dan imbasan tomografi terkomputer (CT). Potensi zeta sasaran - 46.125 mV dicapai dalam keadaan optimum 10 ml  $\text{HAuCl}_4$ , 30 ml SC dan amplitud sonikasi 40%, yang konsisten (sekitar 99.2%) dengan potensi zeta purata sebenar (- 45.8 mV). Kestabilan dan mono menyuraikan  $\text{Fe}_3\text{O}_4$  NPs meningkat setelah pengubahsuaian menjadi  $\text{Fe}_3\text{O}_4@Au$ , seperti yang ditunjukkan oleh peningkatan potensi zeta dari - 24.2 mV menjadi - 45.8 mV. Nilai kemagnetan tepu ( $M_s$ )  $\text{Fe}_3\text{O}_4$  adalah 54 emu / g, sementara nilai  $\text{Fe}_3\text{O}_4@Au$  NP adalah 38 emu/g.  $\text{Fe}_3\text{O}_4@Au$  NP menunjukkan keserasian bio yang baik dan potensi besar sebagai agen kontras mod dua untuk pencitraan MRI / CT. Nilai kelonggaran melintang dan pelemahan sinar-X dari NP yang disintesis ( $222,28 \text{ mM}^{-1} \text{ s}^{-1}$  dan  $HU = 418$ ) lebih besar daripada nilai NP yang disediakan menggunakan kaedah konvensional dan NP komersial. Karya ini menunjukkan kemajuan yang cukup besar pada  $\text{Fe}_3\text{O}_4@Au$  NP dengan memberikan kaedah yang mudah dan pantas untuk mensintesis  $\text{Fe}_3\text{O}_4$ NPs bersalut Au berkualiti tinggi.

**IRON OXIDE ENCAPSULATED GOLD COLLOIDAL NANOPARTICLE  
VIA RAPID SONOCHEMICAL METHOD FOR MRI AND CT IMAGING  
APPLICATION**

**ABSTRACT**

Core@shell nanoparticles ( $\text{Fe}_3\text{O}_4@Au$  NPs) have multiple functions obtained in one stable entity and thus have been extensively investigated. Combining  $\text{Fe}_3\text{O}_4$  and Au NPs in one core@shell nanostructure is a promising strategy for diagnostic biomedical applications. However, the conventional direct methods for  $\text{Fe}_3\text{O}_4@Au$  NPs synthesis are laborious and time-consuming. Therefore, this study presents a facile and rapid sonochemical technique of synthesising  $\text{Fe}_3\text{O}_4@Au$  NPs with excellent physicochemical properties for magnetic resonance imaging (MRI) and computed tomography (CT) scan. The Au shell is coated on  $\text{Fe}_3\text{O}_4$  NPs using a Vibra-Cell ultrasonic solid horn with tip size, frequency and power output of ½ inch, 20 kHz and 750 watts, respectively within 10 minutes. The targeted zeta potential of - 46.125 mV was achieved under the optimum conditions of 10 ml of  $\text{HAuCl}_4$ , 30 ml of sodium citrate (SC) and sonication amplitude of 40%, which is consistent (about 99.2%) with the actual average zeta potential (- 45.8 mV). The stability and monodispersing of  $\text{Fe}_3\text{O}_4$ NPs improved following modification to  $\text{Fe}_3\text{O}_4@Au$ , as indicated by the increase in zeta potential from - 24.2 mV to - 45.8 mV. The saturation magnetization ( $M_s$ ) value of  $\text{Fe}_3\text{O}_4$  was 54 emu/g, while that of  $\text{Fe}_3\text{O}_4@Au$  NP is 38 emu/g. In general, the sonochemical method effectively synthesis highly stable and monodisperse  $\text{Fe}_3\text{O}_4@Au$  NPs with an average size of about 20 nm within 10 minutes. The  $\text{Fe}_3\text{O}_4@Au$  NPs showed good biocompatibility and great potential as a dual-mode

contrast agent for MRI/CT imaging. The transverse relaxivity values and X-ray attenuation of the as-synthesised NPs ( $222.28 \text{ mM}^{-1} \text{ s}^{-1}$  and  $\text{HU} = 418$ ) are greater than those of NPs prepared using conventional methods and commercial NPs. This work reveals considerable progress on  $\text{Fe}_3\text{O}_4@ \text{Au}$  NPs by providing a facile and rapid method to synthesise high-quality Au-coated  $\text{Fe}_3\text{O}_4$  NPs. Importantly, the results demonstrate that all the objectives set for this thesis have been achieved.

# CHAPTER 1

## INTRODUCTION

### 1.1 History of Nanotechnology

The term “nanotechnology” was first introduced by Prof. Norio Taniguchi in 1974 [1]. However, the concept of “smallness” already evolved from its early inception when a Nobel Prize winner in Physics, Richard Feynman, presented the speech titled "There's Plenty of Room at the Bottom" at an American Physical Society meeting at Caltech in December 29, 1959 [2]. The presentation explored the prospect of directly manipulating discrete atoms as a more potent tool in chemical synthesis than the conventional approaches. Modern nanotechnology was launched with the manufacture of a scanning tunnelling microscope (STM), which is capable of visualizing individual atoms. According to the Oxford English Dictionary, nanotechnology is defined as “A branch of technology that focuses on tolerances and dimensions lower than 100 nanometres, particularly the manipulation of discrete atoms and molecules”.

An intrinsic aspect of nanotechnology is that the physicochemical properties of nanoscaled materials varies highly from those of bulk materials with similar composition. For example, bulk gold material is recognized to be inert and unreactive as a catalyst, whereas gold nanoparticles exhibit a remarkably high catalytic reactivity in a wide array of reactions that include carbon monoxide and alcohol oxidation in the gas phase [3]. Another example for nanomaterials displaying differences in their properties from their bulk materials is non-magnetic bulk materials including Pt, Au and Pd nanomaterials embedded in polymer display magnetic moments at nanometric size of nanomaterials, whereas their bulk counterparts are non-magnetic [4, 5]. Two factors can attribute this variation in physicochemical properties reasons: (1) surface effect of the nanomaterials, where the fraction of atoms at the surface have fewer

adjacent atoms compared to their bulk counterpart and (2) quantum effects that show discontinuous behaviour, which is attributable to the completion of shells in systems by delocalized electron [6]. Due to these distinctive properties, nanomaterials are extensively applied in many fields like electronics, energy, telecommunication and biomedical applications. The nanomaterials utilized for biomedical research and development applications comprise liposomes, polymeric micelles, block ionomer complexes, dendrimers, quantum dots and inorganic nanoparticles such as silica, gold and superparamagnetic iron oxide nanoparticles [7].

### **1.2 Iron Oxide Nanoparticles ( $\text{Fe}_3\text{O}_4$ NPs)**

$\text{Fe}_3\text{O}_4$  NPs are inorganic materials with diameters ranging from 1 to 100 nm.  $\text{Fe}_3\text{O}_4$  with a grain size of smaller than 20 nm display superparamagnetic behaviour (ability to have zero magnetism in the absence of external magnetic field) at high temperatures, since after the absence of the magnetic field, their magnetization will disappear, thus preventing the possible agglomeration and embolization of the capillary vessels [8]. Furthermore, these particles exhibit no coercivity and remanence at room temperature [9, 10].  $\text{Fe}_3\text{O}_4$  NPs are extensively utilized in several biomedical applications such as Magnetic Resonance Imaging (MRI), Computed Tomography (CT), drug delivery, biosensors, and hyperthermia [11]. The use of  $\text{Fe}_3\text{O}_4$  nanoparticles in these applications is based on their relatively low toxicity, slow oxidation, high saturation magnetization, and higher magnetic susceptibility compared to maghemite ( $\gamma\text{-Fe}_2\text{O}_3$ ) [12].

### **1.3 Core@shell Nanoparticles ( $\text{Fe}_3\text{O}_4$ @Au NPs)**

Surface modification of  $\text{Fe}_3\text{O}_4$  NPs with a suitable shell is a necessary action for the various application of  $\text{Fe}_3\text{O}_4$  for two reasons: (i) being nanometer sizes, the

ratio of the surface to volume makes them highly active which require surface modification to minimize the surface energy for keeping the appropriate chemical stability, (ii) the advantages of  $\text{Fe}_3\text{O}_4$  NPs become available only when it is well dispersed in the solution; therefore, the modification is effective to prevent the agglomeration. Au shell is considered the most viable option for fabricating magnetic core@shell NPs because it is biocompatible, chemically stable, and possesses exceptional optical characteristics and non-complex biofunctionalization. The rapid magnetic responsiveness of the magnetic core and exceptional biocompatibility of Au shell enable conjugation with relevant biomolecules as well as ensure their applicability in the biomedical field [13-18].

#### **1.4 Problem statement**

Numerous methodologies have been employed to synthesise  $\text{Fe}_3\text{O}_4$  core coated with Au shell. One example is a direct coating, which is simple but involves a difficult process of combining two seemingly incompatible surfaces. The results usually indicate poor dispersion and thus fail to produce  $\text{Fe}_3\text{O}_4$ @Au NPs [19]. Additionally, the process is laborious and time-consuming [20], hindering the irregular shape and also the size of more than 100 nm, resulting in an undesired effect on their biomedical applications [21]. The efficacy of the nanoparticles for biomedical application depends on their stability and biocompatibility [22]. The stability of the NPs and consequently, their nanoscale size is also paramount for their elimination/excretion out of the organism after the diagnostic. Hence, to reach and pass clinical tests with NPs, the right choice of the coating matters because this ultimately enables NPs to fulfil their task in the complex environment of biological fluids, cells and organisms [23]. In addition, the toxicity of NPs has been shown to be dependent on their stability [24],

which has also led to a need to understand the behaviour of NPs suspensions to be settled. Importantly, the nanoparticles, which change particle stability over time, could potentially cause toxic effects [25]. A few studies have been reported for synthesis  $\text{Fe}_3\text{O}_4@Au$ NPs using a sonochemical method but still, there is a lack of stability measurement as well as the use of  $\text{Fe}_3\text{O}_4@Au$ NPs for medical applications that sonochemically synthesised [26-28]. In addition, modern optimization protocols (individually) are unable to predict the relationship between variables and time-consuming procedures requiring multiple experiments and the use of toxic chemicals [29]. The advantage of the response surface methodology (RSM) is its ability to handle variables ( $\text{HAuCl}_4$ , sodium citrate (SC), and sonication amplitude) and response (zeta potential) without the limitations mentioned above [30], this enables the development of an appropriate predictive model capable of correlating responses to multiple factors, even in cases of complex interactions [31]. Despite the numerous applications by RSM for the optimization of experimental procedures [32-35], this study is the first to combine RSM with zeta potential to systematically investigate the influence of the sonochemical effect on the surface functionalization process.

In this research, a rapid and simple sonochemical approach was explored to synthesise  $\text{Fe}_3\text{O}_4@Au$ NPs with unique physiochemical features such as good monodispersed, uniformity, stability, biocompatibility and potential application as a dual-mode contrast agent for MRI and CT imaging in a short time. Therefore, this work was also aimed to optimize the sonochemical conditions for the effective Au coating of  $\text{Fe}_3\text{O}_4$  core NPs for the synthesis of highly stable  $\text{Fe}_3\text{O}_4@Au$  NPs via a sonochemical approach. Using RSM, various parameters were used to optimize the zeta potential value of as-synthesised  $\text{Fe}_3\text{O}_4@Au$  NPs such as gold precursor, sodium citrate and the sonication amplitude. One parameter was fixed at its optimum level for

a single run, whereas the other two parameters were varied within their experimental ranges.

### **1.5 Objective of the study**

The main objectives of this report are summarized in the points below:

1. To synthesis a highly stable  $\text{Fe}_3\text{O}_4@Au$ NPs using sonochemical method in a short time.
2. To optimize the synthesised  $\text{Fe}_3\text{O}_4@Au$ NPs via RSM and investigate the interaction effects among the independent variables on response.
3. To evaluate the physicochemical properties and their toxicity of  $\text{Fe}_3\text{O}_4$  and  $\text{Fe}_3\text{O}_4@Au$ .
4. To evaluate the sensitivity of the  $\text{Fe}_3\text{O}_4@Au$  NPs prepared under optimum synthesis parameters for application as a dual-mode contrast agent for MRI and CT imaging.

### **1.6 Scope of the study**

The scope of this study is limited the preparation of  $\text{Fe}_3\text{O}_4$  core coated with Au shell to generate highly stable  $\text{Fe}_3\text{O}_4@Au$ NPs using a sonochemical method in a short time. The optimization process was based only on response surface methodology (RSM). The frequency/power of the ultrasonic probe is limited to 20 kHz/750 watts in 10 minutes. MRI and CT used only agar phantom with  $\text{Fe}_3\text{O}_4@Au$ NPs as a dual-mode contrast agent.

## **1.7 Contribution of the study**

This study contributes on the new knowledge about a rapid and simple sonochemical approach to synthesise  $\text{Fe}_3\text{O}_4@Au\text{NPs}$  with high stability and biocompatibility acting as a dual-mode contrast agent for MRI and CT imaging in a short time.

This study also contributes to the subject of optimizing the sonochemical conditions for the effective Au coating of  $\text{Fe}_3\text{O}_4$  core NPs using RSM.

## **1.8 Organization of the thesis**

This thesis comprises of six chapters. The introduction, problem statement, objectives and aims of this thesis are presented in Chapter 1. Literature review on synthesis of  $\text{Fe}_3\text{O}_4$ ,  $\text{Fe}_3\text{O}_4@Au\text{NPs}$  and surface modification with different organic and inorganic are presented in Chapter 2. The various theories used to support this research are presented in Chapter 3. The whole experimental procedures, characterisation techniques and optimization of the as-synthesised  $\text{Fe}_3\text{O}_4@Au\text{NPs}$  for application as a dual-mode contrast agent for MRI and CT imaging are described in chapter 4. Details of the various results observed in this work are highlighted and discussed in Chapter 5. The conclusion and future work of this thesis is presented in Chapter 6.

## **CHAPTER 2**

### **LITERATURE REVIEW**

#### **2.1 A brief overview of iron oxide nanoparticles**

In recent times, magnetite nanoparticles ( $\text{Fe}_3\text{O}_4$  NPs) have been comprehensively researched because of their extensive biomedical uses, e.g. cancer treatment, drug delivery, hyperthermia therapy and dual-mode contrast agent for MRI and CT scan.  $\text{Fe}_3\text{O}_4$  NPs ( $\leq 20$  nm) possess exceptional properties that include biocompatibility, non-toxicity, good magnetic susceptibility and superparamagnetic behaviour [9, 36]. Superparamagnetic behaviour is an essential characteristic of  $\text{Fe}_3\text{O}_4$ , since, after the absence of an external magnetic field that applies to  $\text{Fe}_3\text{O}_4$ , their magnetization will disappear (zero magnetism), preventing the possible agglomeration and embolization of capillary vessels [8].

#### **2.2 Wet chemical methods for the synthesis of magnetite nanoparticles**

There are several widely reported chemical methods for the synthesis of  $\text{Fe}_3\text{O}_4$  nanoparticles for biomedical applications, namely co-precipitation, electrochemical, hydrothermal, microemulsions and reverse micelles, sol-gel, solvothermal, sonication and thermal decomposition. In general, all agree that the synthesis of  $\text{Fe}_3\text{O}_4$  nanoparticles is a complicated process due to their colloidal nature. The advantages, disadvantages, and features of the obtained  $\text{Fe}_3\text{O}_4$  products from each method are summarized in Table 2.1. These methods' main challenges consist of determining the experimental conditions for synthesising monodisperse of  $\text{Fe}_3\text{O}_4$  grains with the desired size. These chemical methods have been successfully employed to synthesis nanoparticles with narrow size distribution and homogeneous composition. Figure 2.1

shows extensive synthesis methods of  $\text{Fe}_3\text{O}_4$  nanoparticles along with its surface modifications.

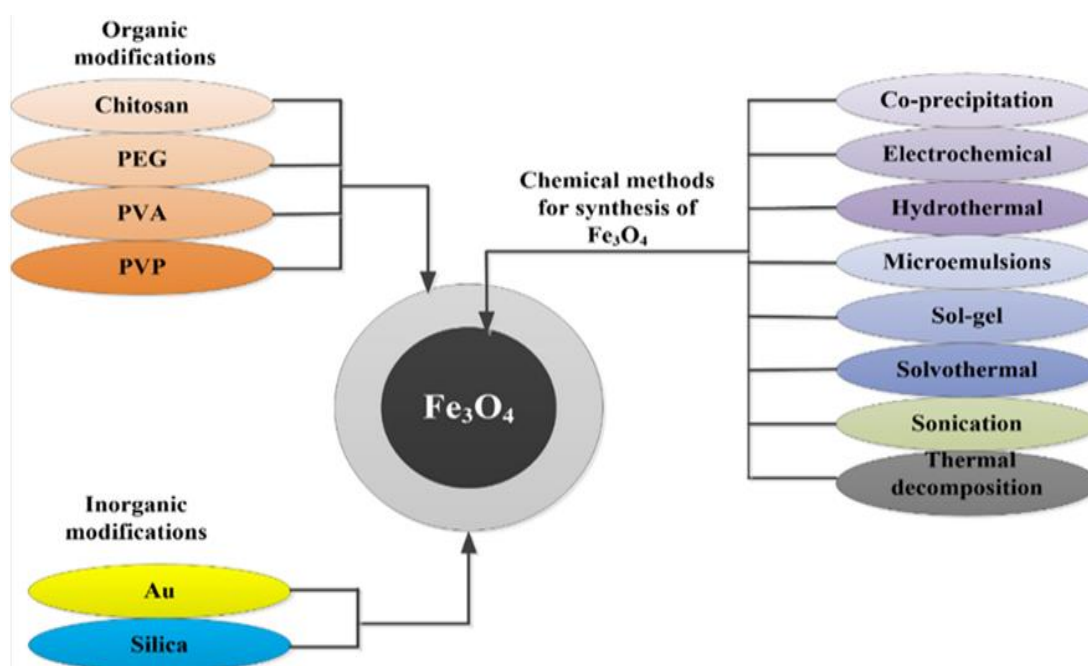


Figure 2.1 Various methods of producing  $\text{Fe}_3\text{O}_4$  and its surface modifications with organic and inorganic materials

### 2.2.1 Co-precipitation method

The co-precipitation method is one of the most important and common chemical wet methods for the preparation of  $\text{Fe}_3\text{O}_4$  in addition to controlling the size and shape of the aqueous solution because its unique features, which include simplicity, ability to be up scaled to a large-scale production, ability to synthesize hydrophilic compounds, and the possibility of being performed at room temperatures [37]. It is also the simplest chemical reaction to produce superparamagnetic iron oxide nanoparticles, SPIONs [38]. A strong base solution such as  $\text{NaOH}$ ,  $\text{NH}_4\text{OH}$  and  $\text{KOH}$  are added to the solution to facilitate the chemical process at room temperature [39], while a weak base such as  $\text{Na}_2\text{CO}_3$  is used for a very slow reaction [40]. The preparation of  $\text{Fe}_3\text{O}_4$  via the co-precipitation method involves the reaction between ferric and ferrous with at ratio 2:1 or 1:1 with vigorous stirring in an aqueous media [41]. The type of precipitating agent

plays a significant role in determining the physicochemical and magnetic properties of Fe<sub>3</sub>O<sub>4</sub> nanoparticles [42]. When strong alkaline media such as LiOH, KOH, and NaOH are used as hydrolyzing agents, an impurity such as Goethite ( $\alpha$ -FeO(OH)) is observed but virtually absent when ammonia (NH<sub>3</sub>) is utilized [43]. The impurity affects and contributes to a decrease in the particles' magnetic moment [44]. Several organic materials served as a peptizing agent in Fe<sub>3</sub>O<sub>4</sub> nanoparticle syntheses such as Citric acid (C<sub>6</sub>H<sub>8</sub>O<sub>7</sub>), nitric acid (HNO<sub>3</sub>), perchloric acid (HClO<sub>4</sub>), and tetramethylammonium hydroxide (C<sub>4</sub>H<sub>13</sub>NO) to prevent agglomeration of Fe<sub>3</sub>O<sub>4</sub> nanoparticles by electrostatic repulsion [45]. Eventually, these substances are incompatible with biomedical applications because they possess an unacceptable percentage of toxicity.

Previous studies have shown that the size of Fe<sub>3</sub>O<sub>4</sub> particles can be controlled by adjusting the reaction conditions such as reaction time, the ratio of concentration Fe<sup>2+</sup>/Fe<sup>3+</sup>, pH, temperature, ionic strength in the medium and stirring speed [45, 46]. The saturation magnetization is directly proportional to the size of the Fe<sub>3</sub>O<sub>4</sub> where the magnetism will decrease when the particle size is small [47]. The main drawbacks of the co-precipitation method are the agglomeration and polydisperse of Fe<sub>3</sub>O<sub>4</sub> nanoparticles. However, recently many researchers have revealed that polymers' presence in chemical reactions can assist a successful synthesis of highly monodisperse and non-agglomeration Fe<sub>3</sub>O<sub>4</sub> particles via steric repulsion [48, 49]. In other words, the polymer works to separate the nucleation and growth process as a capping agent and prevents growth after the process of nucleation. The co-precipitation used NaOH can be easily implemented and requires less time and has the highest yield. Nonetheless, the same cannot be said about when NH<sub>3</sub>.H<sub>2</sub>O is used. Results show that smaller size and low output yield were obtained, and longer synthesis time was required [50]. During the preparation process, it is preferable to have an N<sub>2</sub> gas to protect the product from

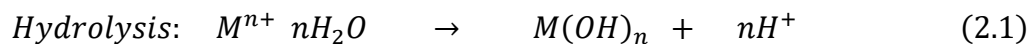
oxidation with the desired temperature. At the end of the process, according to previous studies, a quick visual indicator for good Fe<sub>3</sub>O<sub>4</sub> is black [51].

### 2.2.2 Electrochemical method

The electrochemical process of producing superparamagnetic iron oxide nanoparticles (SPIONs) is based on oxidation and reduction reaction of iron which base electrolyte's in an electrolyte. The electrochemical method has also been utilized to generate various Fe<sub>3</sub>O<sub>4</sub> nanoparticles phases such as magnetite (Fe<sub>3</sub>O<sub>4</sub>) and maghemite (Fe<sub>2</sub>O<sub>3</sub>) nanoparticles [52]. This phenomenon can be explained by crossing an electric current through two electrodes (anode and cathode). More so, the positively charged electrode (anode) can be oxidized to metal ion species inside the electrolyte and the metal ion is later reduced to metal by the negatively charged electrode (cathode) with the assistance of stabilizers. The Fe<sub>3</sub>O<sub>4</sub> nanoparticles are generally deposited on the electrode generally in a coating or thin film. The synthesis of Fe<sub>3</sub>O<sub>4</sub> nanoparticles via this method does not require high temperature and the electrolyte's temperature must be less than the boiling point. This method has a disadvantage at room temperature, often produces poorly ordered particles that cause an explicit structural characterization hard [53].

### 2.2.3 Hydrothermal method

A hydrothermal method is one of the most common wet chemical ways for the synthesis of inorganic nanocrystals, especially for metal and metal oxides [54, 55]. The formation of Fe<sub>3</sub>O<sub>4</sub> nanoparticles involves two steps; firstly, the hydrolysis reaction, and then the dehydration process, as demonstrated in Equation (1) and (2) [56].



This method often utilizes relatively high temperature and pressure to influence the formation of nanocrystals. It includes the heating of a water solution of iron salt at a temperature and pressure of 374 ° C and 22.1 MPa, respectively. The hydrothermal process has various advantages such as facile control, environmentally friendly process, good crystallization and morphology of products. In addition, under this high pressure, some metastable and condensed phases can be produced. Different shapes of Fe<sub>3</sub>O<sub>4</sub>NPs have been prepared via hydrothermal syntheses, such as nanorods, nanowires, nanospheres and many other shapes [57-59]. Fe<sub>3</sub>O<sub>4</sub> nanoparticles with an average of 50 nm have been prepared by utilizing Na<sub>2</sub>S<sub>2</sub>O<sub>3</sub> as the control agent via the hydrothermal method.

The synthesising of the Fe<sub>3</sub>O<sub>4</sub> nanoparticles phase depends on the ratio of Na<sub>2</sub>SO<sub>3</sub> to FeSO<sub>4</sub> [60]. Fe<sub>3</sub>O<sub>4</sub> nanoparticles with size 27 nm in the presence of a suitable surfactant via hydrothermal process have been prepared [61]. Previous studies demonstrated that microwave hydrothermal with a temperature range of 90 to 200°C had demonstrated spherical Fe<sub>3</sub>O<sub>4</sub> nanoparticles with sizes ranging between 150-200 nm by using the FeCl<sub>3</sub>.FeSO<sub>4</sub>.7H<sub>2</sub>O as precursors and NaOH as hydrolysis reactant. It was found the formation of Fe<sub>3</sub>O<sub>4</sub> nanoparticles controlled by a critical parameter (Fe/NaOH). Chen et al. reported that Fe<sub>3</sub>O<sub>4</sub> nano-powders prepared via a hydrothermal process by employ Fe<sup>2+</sup> precursor (FeCl<sub>2</sub>·4H<sub>2</sub>O). They used the FeCl<sub>2</sub> to react with the mixing of N<sub>2</sub>H<sub>4</sub> and NaOH; thus, the iron salts Fe<sup>2+</sup> and Fe<sup>3+</sup> had partially oxidized by N<sub>2</sub>H<sub>4</sub> [62].

The hydrothermal method also used the Polyvinylpyrrolidone (PVP) as the surfactant where the shape of Fe<sub>3</sub>O<sub>4</sub> nanoparticles can be controlled by mixing FeSO<sub>4</sub>.7H<sub>2</sub>O, NaOH, FeCl<sub>3</sub> with benzene and PVP. By varying PVP amount and

experimental conditions,  $\text{Fe}_3\text{O}_4$  nanoparticles with different morphologies can be obtained, like nanowires, nanorods, nanoparticles and mixtures [63]. However, the disadvantage of this method is the slow reaction kinetics at any proposed temperature. Therefore, microwaves assisted hydrothermal process was proposed [64]. The microwave heating process provides increased interaction kinetics and improved crystallization of the sample. By combining of two process hydrothermal effects and microwave irradiation, the morphology of synthesised SPIONs can be adjusted or controlled. SPIONs with cubical shaped or rhombohedral, hexagonal were reported [65]. In this study, the hydrothermal method recorded many advantages features such as high yield, controllable size, excellent particle crystallinity and good morphology [66].

#### **2.2.4 Microemulsions and reverse micelles method**

A stable or thermodynamically stable system consists of two liquids immiscible such as oil and water in addition to the presence of surfactant aggregate [66]. There are three types of microemulsions; firstly, direct oil in water microemulsion (o/w), secondly, reversed water in oil (w/o), and thirdly, bicontinuous. This classification depends on the hydrophilic-lipophilic balanced value and water ratio to oil (w/o) [67]. Nanoparticles formation under the microemulsion method undergoes four phases. I), mixing of microemulsion components II), exchange of substances through the nano-droplets, III) reaction nucleation and IV), reaction outgrowth [68]. Particle stability via this method is influenced by the amount and type of surfactant, and the pH of the dispersing medium [69].

As demonstrated in Figure 2.2, when two nanoparticles collided together, the reactants would be exchanged for the formation of nanoparticles by the Brownian movement [70]. A water droplet covered with a suitable surfactant is called a

nanoreactor. More importantly, the surfactant prevents water droplets from forming excess aggregation [71]. A study has recently demonstrated that the microemulsion process can synthesis monodisperse SPIONs by varying the concentration of precursor and size of the droplet radius, as shown in Figure 2.3d [72]. SPIONs can be prepared through two methods firstly, water in oil (w/o) and the second oil in water (o/w) via microemulsions process [73]. The conventional method of synthesis SPIONs via microemulsion need to add reducing agent such as ammonia to reactants [74]. The size distribution and shape can be controlled by manipulation in the amount of surfactant, water and oil via microemulsion process [75], while using different temperatures during the reaction produced  $\text{Fe}_3\text{O}_4$  nanoparticles with a diameter in the range of 3 to 12 nm [76]. Jia et al. reported a new procedure by adding basic solution NaOH as a reducing agent to produce  $\text{Fe}_3\text{O}_4$  surrounded by chitosan. This component's size ranged from 10-80 nm [77]. Like the problem observed in the co-precipitation method, the main disadvantage is the agglomeration and inability to monodispersed the particles and precisely control the size. Furthermore, a large amount of dissolvent is necessary to synthesis a ratable amount of nano-materials and to reverse the effects of residual surfactants on the property of the particles [78]. In order to overcome those limitations, oleic acid can be added to the reactants as stabilizing agents [79]. This method's main advantage is that it is environmentally friendly and economical [80]. More importantly, the SPIONs synthesised via this method depends on droplet size, surfactant and the concentration of reactant [81].

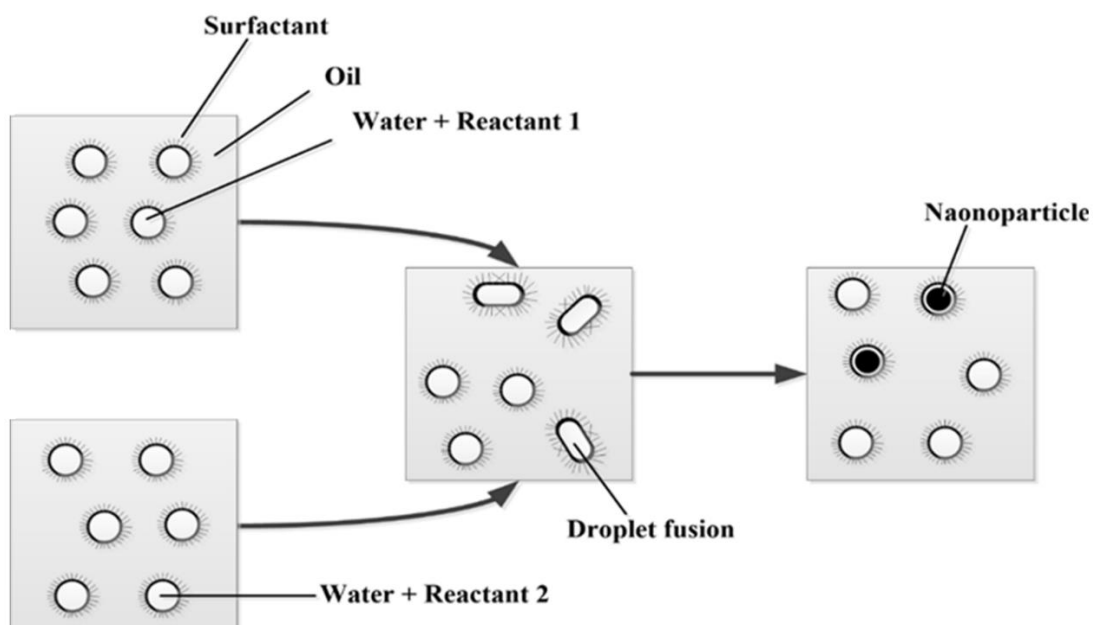


Figure 2.2 The formation of  $\text{Fe}_3\text{O}_4$  NPs by mixing two water-in-oil microemulsions, where reactant 1 contains salt or a complex of a metal, while reactant 2 contains a precipitating agent [82]

### 2.2.5 Sol-gel method

In wet chemical approaches, sol-gel is one technique for producing  $\text{Fe}_3\text{O}_4$  nanoparticles with unique properties, which involves hydroxylation and condensation of precursors turn into an inorganic solid [83].  $\text{Fe}_3\text{O}_4$ , prepared via sol-gel, is very high purity and homogeneous [84]. The morphology and structure can be adjusted by adjusting the parameter, such as the salt precursors' concentration, pH, agitation, and temperature [85]. However, the change in pH also affects the magnetic properties of the resulting materials [86]. There are four steps in synthesising  $\text{Fe}_3\text{O}_4$  nanoparticles using this method; (a) hydrolysis and poly-condensation of iron precursor in a solvent to form a colloidal suspension of the particles (sol), (b) gelation of the sol to form a gel, (c) the aging and (d) drying of the particles. Nevertheless, similar to the co-precipitation process, the sol-gel is challenged to produce monodisperse particles and prevent agglomeration. Several improvements have been reported to the synthesis of

monodisperse and non-agglomerated via the sol-gel process to overcome both limitations. Dong and Zhu. have been recorded that polyethylene glycol (PEG) can be used as a capping agent to mitigate the agglomeration and give the uniform size of  $\text{Fe}_3\text{O}_4$  nanoparticles [87]. The sol-gel method has been prepared to synthesis nanocomposite materials by using aqueous methods [88]. The method used in this study has several merits. Firstly, its ability to monitor the fine structure identity of the reaction outputs. Secondly, its ability to get a pure amorphous stage, solo-dispersity, and well monitoring of the particle diameter. Thirdly, it is possible to get items with a prearranged shell regarding empirical situations.

#### **2.2.6 Solvothermal method**

A solvothermal method involves presenting the organic solvent like ethanol, methanol or polyol at an extremely high temperature and pressure [89]. Recently, many authors demonstrated that SPIONs had been synthesised by a solvent such as hydrazine ( $\text{N}_2\text{H}_4$ ) and ethylenediamine ( $\text{C}_2\text{H}_8\text{N}_2$ ) [90, 91]. The morphology and good uniformity in this method result from the reaction between the iron precursor and surfactant [92]. J. Liang et al. have been demonstrated that the size of  $\text{Fe}_3\text{O}_4$  nanoparticles can be controlled by changing the ratio of surfactant, the concentration of NaOH, and precipitator [93]. In the solvothermal technique, the dispersity of iron salts, the temperature of reaction and the aging time are crucial parameters in determining the size distribution and controlling the nucleation and growth processes [94, 95]. Various surfactants such as sodium dodecyl benzene sulfonic, polyacrylic acid [93], and oleic acid [96] have been utilized as capping agents to preparation  $\text{Fe}_3\text{O}_4$  nanoparticles with high monodispersity. The  $\text{Fe}_3\text{O}_4$  nanoparticles that were prepared by this method are hydrophilic, which can be dispersed in an aqueous solution or polar solvents [97]. This

method's advantages include no requirement for any surfactant or reducing agents except liquid polyols and control experimental conditions [98].

### **2.2.7 Sonication method**

Sonication method (sonochemical or sonolysis) is a facile way to synthesis SPIONs and other nanostructure by decomposition (sonolysis) of an inorganic iron precursor using very high temperature and pressure generated by ultrasonic irradiation, up to 5000 K and 1000 atm, respectively [99]. The ultrasonic irradiation produces high temperature leads to generates magnetic nanoparticles by decomposition iron salts [100]. Hydrophilic and monodisperse properties of SPIONs have been improved via sonication method [101]. Recently, many authors reported the presence of a suitable stabilizer to contribute to synthesis SPIONs with high dispersed via ultrasonic irradiation [102, 103]. The sonication method often produces an amorphous shape because of the high temperature and pressure resulting from this process [104, 105]. More importantly, during the formation process of SPIONs, the acoustic cavitation process inhibits crystallization. More so, the crystalline properties of the SPIONs can be controlled by heat treatment [105].

The synthesising of SPIONs with crystalline properties at low ultrasonic temperature also has been recorded [106]. Sonication method for synthesising Fe<sub>3</sub>O<sub>4</sub> NPs depends on a number of parameters, such as temperature, time, sonication frequency, to control size distributions and morphology [105].

### **2.2.8 Thermal decomposition method**

The thermal decomposition technique is a well-known process for synthesising monodisperse and highly crystalline of SPIONs [107]. It involves the decomposition of iron precursors by very high temperatures [108]. In addition, the crystallinity and

magnetic properties of SPIONs can be obtained by increasing the mixture reaction up to 300°C [109]. During the thermal decomposition process, the nanoparticles undergo two important routes for control nucleation and growth mechanization. Firstly, involve direct injection of organometallic compounds in hot surfactant solution that results in the immediate formation of nuclei. Secondly, involves control heating of these compounds in surfactant solution for nuclei formation [110]. Park et al., Roca et al. and Baaziz et al. have reported that the precursor concentrations and the ratio of Fe/oleic acid are as critical parameters in controlling nanoparticles size [111-113]. A high-temperature reaction of Fe<sub>2</sub>O<sub>3</sub> acetylacetonate with 1,2-hexadecanediol in existence oleylamine and oleic acid is needed to acquire monodisperse magnetite nanoparticles. In presence of a bipolar surfactant, the hydrophobic nanoparticles can be converted into hydrophilic and the diameter of particles also tuned from 4-20 nm [114]. N.R. Jana et al and M. Mohapatra et al have been proposed the use of non-toxic FeCl<sub>3</sub> and FeCl<sub>2</sub> salts as a precursor [115, 116].

Recently, the thermal decomposition method producing a water-dispersible magnetic nanoparticle in acidic has been synthesised using FeCl<sub>3</sub> and Fe(acac)<sub>3</sub> [117]. The diameters nanoparticles of 4,12 and 60 nm can be controlled according to the time of reflux (condensation of vapours and the return of this condensate to the system) [118]. Interestingly, the shape of nanoparticles from spherical to cubic has been changed by increasing reflux time. The synthesis of Fe<sub>3</sub>O<sub>4</sub> via thermal decomposition method requires further investigation on the mechanism of chemical conversions because the reaction mixtures produced contain multicomponent reactions e.g., different kind of components was produced during the oxidative of Fe (II) including iron Fe<sub>3</sub>O<sub>4</sub>,  $\gamma$ -Fe<sub>2</sub>O<sub>3</sub>, FeO, ( $\alpha$ -Fe),  $\alpha$ -Fe<sub>2</sub>O<sub>3</sub>, siderite (FeCO<sub>3</sub>) and iron carbide(Fe<sub>3</sub>C) [119]. The advantages of thermal decomposition are inexpensive iron-organic precursors and very short

reaction time. Thermal decomposition process also has some disadvantages such as complicated procedures [89], emission of toxic gases such CO [120], uses toxic and expensive reagents (not environmentally friendly) [82], required high reaction temperature [89], uses the multiple reagents [89] and the inability to get required nanoparticle size [121]. Future development of this method should strive towards the synthesis of water-soluble magnetic nanoparticles directly that uses less reagents.

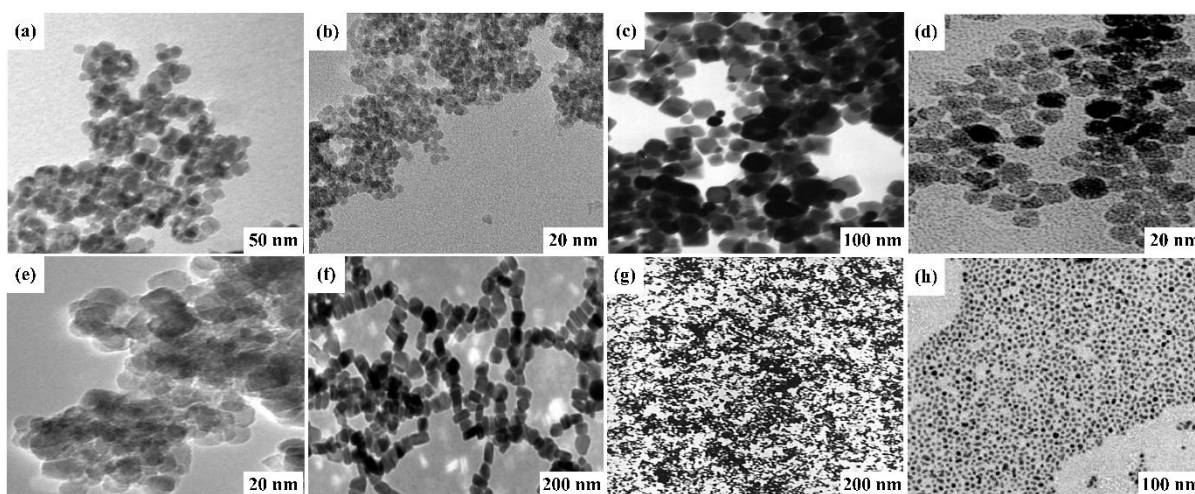


Figure 2.3 TEM images with different sizes and shapes of agglomerated Fe<sub>3</sub>O<sub>4</sub> depending on the method of synthesis (a) Co-precipitation [122] (b) Electrochemical [53] (c) Hydrothermal [62] (d) Microemulsion [70] (e) Sol-gel [123] (f) Solvothermal [91] (g) Sonication [124] (h) Thermal decomposition [125]

Table 2.1 Comparison between synthesis methods in preparation Fe<sub>3</sub>O<sub>4</sub>

<b>Method</b>	<b>Features of the obtained Fe<sub>3</sub>O<sub>4</sub> products</b>	<b>Reaction condition</b>	<b>Advantage</b>	<b>Disadvantage</b>	<b>Yield</b>	<b>Ref.</b>
<i>Co-precipitation</i>	Magnetization value: 20-80 emu/g Size distribution: Broad Shape control: Not good	Temperature: 20-90°C Duration: Minutes	Facile, simple, easy, low cost and controllable size.	Agglomeration and difficulty in avoiding nucleation during the reaction	High	[126]
<i>Electrochemical</i>	Magnetization value: 35.5 emu/g Size distribution: Medium Shape control: Medium	Temperature: Room temp Duration: Hours-days	Facile, high purity and particle size can be controlled	Complex procedure	Medium	[53]
<i>Hydrothermal</i>	Magnetization value: 20-80 emu/g Size distribution: Very narrow / Narrow–broad Shape control: Very good	Temperature: 150-220°C Duration: Hours-days	Facile, crystalline, highly pure and environmentally friendly	The crystal growth cannot be controlled	High	[127]
<i>Microemulsions</i>	Magnetization value: up to 113 emu/g Size distribution: Narrow Shape control: Good	Temperature: 20-50°C Duration: Hours	Uniform and thermodynamically stable nanoparticles	Complex and heterogeneous	Low	[73]
<i>Sol-gel</i>	Magnetization value: 10-40 emu/g	Temperature: 25-200°C Duration: Hours	Desired shape and hybrid nanoparticles	The product contains a sol-gel mixture component	Medium	[128]

	Size distribution: Narrow Shape control: Good					
<i>Solvothermal</i>	Magnetization value: up to 108 emu/g Size distribution: Narrow-broad Shape control: Good	Temperature: 150- 220°C Duration: Hours- days	High Purity, good crystallinity	Relatively slow kinetic and sensitive to the concentrations of alkalinity and water	High	[92]
<i>Sonication</i>	Magnetization value: 63 emu/g Size distribution: Narrow Shape control: Bad	Temperature: 20- 50°C Duration: Minutes	Facile, rapid and environmental friendly	Amorphous nanoparticles	Medium	[129]
<i>Thermal decomposition</i>	Magnetization value: up to 91 emu/g Size distribution: Very narrow Shape control: Very good	Temperature: 100- 320°C Duration: Hours- days	Monodispersed, inexpensive and high quality of Fe <sub>3</sub> O <sub>4</sub> nanoparticles	Complicated and requiring high temperatures	High	[130]

## **2.3 Surface modification of Fe<sub>3</sub>O<sub>4</sub> NPs**

The modification of Fe<sub>3</sub>O<sub>4</sub> nanoparticles surface with organic or inorganic materials can provide biocompatible nanoparticles for biomedical application. Coating Fe<sub>3</sub>O<sub>4</sub> nanoparticles with inorganic materials such as gold and silica nanoparticles gave them many advantages, including high stability and the ability to bind biological molecules to Fe<sub>3</sub>O<sub>4</sub> nanoparticles' surface. On the other hand, if hydrophobic Fe<sub>3</sub>O<sub>4</sub> nanoparticles are coated with organic materials (hydrophilic polymers) such as chitosan, Polyethylene glycol (PEG), Polyvinyl Alcohol (PVA), and Polyvinylpyrrolidone (PVP), the agglomeration of the iron oxide nanoparticles can mostly be avoided.

### **2.3.1 Inorganic coating**

#### **2.3.1(a) Gold**

Gold is an inorganic coating to implement functionality and improve the stability of magnetic nanoparticles in aqueous dispersions. Au coating has a unique feature called surface plasmon resonance (SPR) which provides optical properties. Besides, the coating with Au nanoparticles can also promote organic conjugation via Au-S chemistry. Fe<sub>3</sub>O<sub>4</sub> coated with Au has been reported by several authors [131, 132]. The coating process is obtained by reducing the Au precursor in the existence of iron oxide nanoparticles. The experimental conditions differ according to the Fe<sub>3</sub>O<sub>4</sub> nanoparticle characteristics like size, shape, surface chemistry and the solubility, etc. Here we introduce some brief examples.

Xu et al. reported that magnetic Fe<sub>3</sub>O<sub>4</sub>/Au core/shell nanoparticles can be synthesised by reducing HAuCl<sub>4</sub> at room temperature. However, the work also indicates that the coating process of Au nanoparticles to cover the surface of Fe<sub>3</sub>O<sub>4</sub> is difficult

because of the incompatible chemistry involved. Furthermore, the rapid reduction of  $\text{HAuCl}_4$  will lead to Au nanoparticles' growth rather than of a coating shell. To prevent the rapid reduction, the process utilizes oleylamine as a moderate reduction agent in a chloroform solution to slowly reduce  $\text{HAuCl}_4$  of  $\text{Fe}_3\text{O}_4$  nanoparticles. Additionally, chloroform is a strong solvent and uses as a surfactant that may help the desorption of oleylamine from the surface of  $\text{Fe}_3\text{O}_4$  nanoparticles.  $\text{Fe}_3\text{O}_4/\text{Au}$  core/shell nanoparticles were soluble in a nonpolar solvent due to an oleylamine still capped at the surface. To make  $\text{Fe}_3\text{O}_4/\text{Au}$  water-soluble,  $\text{Fe}_3\text{O}_4/\text{Au}$  core/shell nanoparticles were dried and mixed with cetyltrimethylammonium bromide (CTAB) and sodium citrate. The negative charge on the Au nanoshell surface is due to the surface that may absorb the sodium citrate, which further led double-layer structure with the capping CTAB and a powerful capping can be achieved to replace oleylamine. Under the reducing condition, the shell thickness Au depends on the ratio of  $\text{HAuCl}_4$ . This method not only protects  $\text{Fe}_3\text{O}_4$  from environmental corrosion but also able to manipulate and improve the SPR properties of the core/shell nanoparticles [132].

Zhong et al. reported another method to synthesis  $\text{Fe}_3\text{O}_4/\text{Au}$  core/shell [133]. The method includes  $\text{Au}(\text{Ac})_3$  as a precursor with temperature ranged 180-190°C in the existence of  $\text{Fe}_3\text{O}_4$  nanoparticles, which used the reducing agent such as 1,2-hexadecandiol and surfactants like oleylamine and oleic acid. At high heating temperature, the adsorption process of oleic acid and oleylamine is facilitated from  $\text{Fe}_3\text{O}_4$  nanoparticles' surface. This method employed a centrifuge to select the proper size and separated the small-sized and large-sized core/shell nanoparticles and uncoated  $\text{Fe}_3\text{O}_4$  nanoparticles. In addition, this method can control a combination of thermally activated desorption of the capping layer and deposition of Au on the bare  $\text{Fe}_3\text{O}_4$  surface, and re-encapsulation of the Au surface by the capping agent. The shell

thickness of Au nanoparticles was determined by TEM analysis [134]. After coating, the thiol inter-particle was used to produce thin Fe<sub>3</sub>O<sub>4</sub>/Au core/shell nanoparticles.

### **2.3.1(b) Silica**

Silica (SiO<sub>2</sub>) has been employed as an inorganic coating material for nanoparticle surface modification in the colloid system [135]. Usually, the silica shell over Fe<sub>3</sub>O<sub>4</sub> nanoparticles' surface provides protection against toxicity, prevents the aggregation of Fe<sub>3</sub>O<sub>4</sub> nanoparticles in liquid, and improves the chemical stability [136]. There are two different ways for the stability of silica coatings over Fe<sub>3</sub>O<sub>4</sub> nanoparticles [137]. Firstly, protection of the dipole interaction with the silica shell and secondly since silica is negatively charged so it enhances the Coulomb repulsion of Fe<sub>3</sub>O<sub>4</sub>. The product is formed of Fe<sub>3</sub>O<sub>4</sub> particles coated with silicon and its diameter 300 nm has been examined in the clinic by oral administration, they found it extremely improves the diagnosis of organ boundaries, like lymph nodes and uterus [138, 139].

Three strategies to create magnetic silica nanospheres will be presented. The first strategy depended on the famous Stöber process, which states silica was produced in situ by condensation and hydrolysis of sol-gel precursors like tetraethyl orthosilicate (TEOS) (Figure 2.4) [140]. Xiong et al. have recorded silica colloids filled with SPIONs by this process have been recorded [141]. This study revealed that there are two key factors to determine the final size of the silica colloids type of solvent and the other is the concentration of Fe<sub>3</sub>O<sub>4</sub> nanoparticles. The second strategy implicates a deposition of silica from the silicic acid solution [142]. Several researchers have demonstrated the silica acid seems to be more effective than TEOS method in covering the Fe<sub>3</sub>O<sub>4</sub> surface [143]. This method is easy and the particle size can be controlled by varying the ratio of Fe<sub>3</sub>O<sub>4</sub> or SiO<sub>2</sub> [144]. The third strategy was about an emulsion way, in which micelle or inverse micelle is used to limit and control the coating of silica wherein the separation

of core/shell nanoparticles from the surfactant is associated with an emulsion system [145]. For instance, Yang et al. have employed this technique in the preparation of silica-coated SPIONs with monodisperse and increased the entrapment of biological molecules in the nanoparticles [138].

Tartaj et al. used a pyrolysis method for coating magnetic sphere aerosol by silica [146]. Gao et al. used seeds hydrophilic  $\text{Fe}_3\text{O}_4$  nanoparticles with size 20 nm used to prepare  $\text{Fe}_3\text{O}_4/\text{SiO}_2$  core/shell nanoparticles and the thickness of a  $\text{SiO}_2$  shell may be tuned from 12.5-45 nm by varying the experimental conditions.

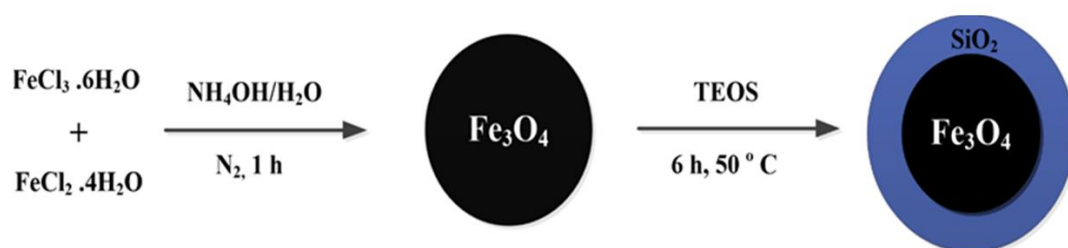


Figure 2.4 Reaction steps of preparation  $\text{Fe}_3\text{O}_4/\text{SiO}_2$  core/shell nanoparticles by condensation and hydrolysis of sol-gel precursors like tetraethyl orthosilicate (TEOS) [147]

### 2.3.2 Organic coating

#### 2.3.2(a) Chitosan

Chitosan is a biopolymer that has immense structural opportunities for mechanical and chemical modifications to produce novel features, application and functions, especially in the biomedical section. It is hydrophilic, non-toxic, non-antigenic, biodegradable and biocompatible polymer [148]. These days, the synthesising of  $\text{Fe}_3\text{O}_4$  NPs encapsulated within chitosan are of paramount importance [149]. The presence of hydroxyl and amino on the chitosan would quickly form complexes with  $\text{Fe}_3\text{O}_4$  surface and make them stable, hydrophilic and biocompatible.

The positive charge of amino groups could interact with a negative charge of nucleic acids for MRI and therapeutic gene delivery [150].

Moreover, the use of chitosan would facilitate the flow of particles across cellular barriers as well as opening up a narrow junction between epithelial cells [151]. Until now, this polymer has been used for coating SPIONs to produce an excellent contrast agent for MRI [152]. Hong et al. synthesised chitosan-coated ferrite nanoparticles to be studied as a contrast agent for MRI [153]. The amino groups of chitosan ( $-NH_2$ ) were tied to the particles whereas the hydroxyl groups ( $-OH$ ) remain untied. Consequently, these kinds of particles have slightly positively charged. Due to the existence of Coulomb repulsion between the positive charge particles and the absence of surface or organic solvents in an aqueous solution of coated particles, the solution will remain suspended in a colloidal state. Kim et al. used the sonochemical technique to produce SPIONs. Kim and their group prepared ferrofluids as a contrast agent for MRI. The nanoparticles' surface was coated with a surfactant such as oleic acid and then dispersing these particles in the chitosan [154]. These spherical particles still retained the superparamagnetic behaviour at a size of 15 nm in diameter. Microspheres composed of superparamagnetic iron oxide nanoparticles and chitosan were improved as a novel MRI-detectable embolic material. Furthermore, Lee et al. have successfully synthesised 15 nm size spherical shaped SPIONs by employing the sonochemistry process and then suspended nanoparticles within amino group chitosan to prepare a ferrofluid [155], where SPIONs/chitosan microspheres exhibited a strong improvement in MRI contrast like as ferrofluid in vitro.

### **2.3.2(b) Polyethylene Glycol (PEG)**

PEG is a water-soluble and biocompatible polymer used in numerous applications in medicine. It is working to increase blood circulation's biocompatibility